



HAL
open science

Synergistic Effects of BaTiO₃ /Multiwall Carbon Nanotube as Fillers on the Electrical Performance of Triboelectric Nanogenerator Based on Polydimethylsiloxane Composite Films

Shan Feng, Hanlu Zhang, Delong He, Yiguo Xu, Anne Zhang, Yu Liu, Jinbo Bai

► To cite this version:

Shan Feng, Hanlu Zhang, Delong He, Yiguo Xu, Anne Zhang, et al.. Synergistic Effects of BaTiO₃ /Multiwall Carbon Nanotube as Fillers on the Electrical Performance of Triboelectric Nanogenerator Based on Polydimethylsiloxane Composite Films. *Energy Technology*, 2019, 7 (6), pp.1900101. 10.1002/ente.201900101 . hal-02546474

HAL Id: hal-02546474



<https://hal.science/hal-02546474v1>

Submitted on 25 May 2020

HAL is a multi-disciplinary open access archive for the deposit and dissemination of scientific research documents, whether they are published or not. The documents may come from teaching and research institutions in France or abroad, or from public or private research centers.

L'archive ouverte pluridisciplinaire **HAL**, est destinée au dépôt et à la diffusion de documents scientifiques de niveau recherche, publiés ou non, émanant des établissements d'enseignement et de recherche français ou étrangers, des laboratoires publics ou privés.

Synergistic effects of BaTiO₃/ Multiwall Carbon Nanotube as fillers on the electrical performance of triboelectric nanogenerator based on Polydimethylsiloxane composite films

Shan Feng, Hanlu Zhang, Delong He , Yiguo Xu, Anne Zhang, Yu Liu, Jinbo Bai 

Laboratoire Mécanique des Sols, Structures et Matériaux (MSSMat), CNRS UMR 8579, Ecole CentraleSupélec, Université Paris-Saclay, 8-10 rue Joliot-Curie, 91190 Gif-sur-Yvette, France

E-mail : delong.he@centralesupelec.fr; jinbo.bai@centralesupelec.fr

Keywords: polydimethylsiloxane composite film, filler size, BaTiO₃, multiwall carbon nanotubes, triboelectric nanogenerator

Abstract:

Herein, polydimethylsiloxane (PDMS) composite films containing ϕ BaTiO₃ particles with an average size of 70 nm and 500 nm are prepared and characterized, respectively. Then, triboelectric nanogenerators (TENG) based on the composite films are designed at different BaTiO₃ sizes and mass ratios. In addition, multiwall carbon nanotubes (MWCNT) are also used for uniform dispersion of BaTiO₃ particles in composite films for the TENG device. With the synergistic effects of BaTiO₃/MWCNT fillers, discrete conductive micronetworks surrounded by BaTiO₃ particles form, and then, the effective filler-matrix interface effect in the three-phase composite is enhanced, leading to superior triboelectric output performance, supported by much higher dielectric permittivity and COMSOL simulation. Moreover, the triboelectric output performance of TENG changes with different-sized BaTiO₃ particles. As to BT-70-MWCNT/PDMS composites, with the same mass ratio of BT, the peak output current is always higher than that of BT-500-MWCNT/PDMS. Furthermore, the optimum BT mass ratio of BT-70-MWCNT/PDMS composites is also higher than that of BT-500. With

BaTiO₃ of size 70 nm, the maximum surface charge density is about 160 $\mu\text{C m}^{-2}$ under an optimized mass ratio, whereas it is about 110 $\mu\text{C m}^{-2}$ for BaTiO₃ of size 500 nm.

1. Introduction

The increasing energy crisis and environmental pollution stimulate the development of renewable energies, which contribute to reducing the greenhouse effect and the consumption of ~~an~~ traditional fossil fuels.^[1] As a new type of renewable energy harvesting system, triboelectric nanogenerators (TENG) has been proved as an alternative and promising tool to harvest renewable energy in recent years.^[2] It works by coupling the effect of triboelectrification and electrostatic induction: mechanical energy is converted to electricity by electrostatic induction of polarized charges created by contact electrification.^[3] Due to the inherent capacitive characteristic of TENG,^[4] it is highly desired to achieve higher output power by increasing the relative capacitance (effective ϵ/d value, in which ϵ is the relative permittivity and d is the film thickness).^[5]

Among numerous triboelectric candidate materials, polydimethylsiloxane (PDMS) is commonly used as the negative triboelectric material for its relatively high electron affinity and high flexibility.^[6] However, as the dielectric constant of pure PDMS is in a low level compared to ceramics, the relative capacitance and electrical performance of TENG are limited and desired to be improved. One solution is to develop inorganic/polymer dielectric composites that have both flexibility and high dielectric constant.^[7] From 2015, the effects of dielectric properties of inorganic/polymer composite materials on the triboelectric output performance have been investigated.^[8] In previous studies, different kinds of high dielectric constant fillers, such as TiO₂, SrTiO₃, BaTiO₃,^[8,9] ZnSnO₃,^[10] CaCu₃Ti₄O₁₂(CCTO),^[11] were

added into PDMS to increase the effective ϵ of the composite film. Among them, BaTiO₃ is one of the most attractive fillers for its high dielectric constant and ferroelectric properties. It has been revealed that the physical, interfacial properties and agglomeration degree of ceramic particles would change drastically with a decrease in particle size, due to greatly increased surface atoms.^[12] The dielectric constant of BaTiO₃ particles decreases dramatically as the grain size reduces from micro- to nanoscale ~~nano-level~~ in terms of grain clamping and elastic constant.^[13] It is well known that large interfacial areas between the nanoparticles and polymer would afford high interface volume fraction and charge injection from particle filler to polymer matrix when the particle size shrinks to nanometer scale,^[14] especially nanoparticles (NPs) <100 nm have high surface energy and unique characteristics compared with bulk materials. Because of these factors, the properties of polymer composites strongly depend on the filler size, filler-matrix interface and the loading of filler.^[15]

For triboelectric applications, more research attention has been given to choosing different types of ceramic or conductive fillers, filler loading and surface structure design, rather than considering the filler-matrix interface effect.^[8,11,16-18] Thus, it is desired to clarify the effect of filler size and filler-matrix interface on the triboelectric performance of a BaTiO₃/polymer composite-based TENG. In this article, BaTiO₃/PDMS composite films with two different particle sizes under various BaTiO₃ concentrations were prepared. MWCNTs were also used as a functional material in the composite films and TENG devices. The three-phase composite was a percolation system, in which MWCNTs were uniformly and randomly dispersed in the matrix and surrounded by BaTiO₃, forming discrete microcapacitor structures. This structure can avoid particle agglomeration efficiently and enhance the total

BaTiO₃ filler-matrix interfacial area. The different effective filler-matrix interface areas with the same BaTiO₃ particle mass ratio and the inter-filler distance were calculated. Meanwhile, the influence of different effective filler-matrix interfaces under the same mass ratio on the triboelectric property of TENG was evaluated by measuring the composite permittivity and output triboelectric performance of the TENG device. COMSOL Multiphysics simulation was also demonstrated to confirm the surface potential difference introduced by different effective filler-matrix interface. Results showed that MWCNTs played an important role in enhancing the effective filler-matrix interface effect for triboelectric output performance.

2. Result and Discussion

2.2. Morphology and Structure of BaTiO₃ NPs

Figure 1 shows the morphology and phase analysis results of BaTiO₃ (BT) NPs. From the SEM images, BT NPs show evidently different sizes with average value corresponding to those from insets in Figure 1a, b. Figure 1c shows the Raman spectra of both BT NPs. Tetragonal BT NPs have characteristic peaks around 304, 516 and 716 cm⁻¹, corresponding to [B1, E(TO+LO)], [A1(TO), E(TO)] and [A1(LO), E(LO)], respectively.^[19] Both the Raman spectra have peak around 304 cm⁻¹, which is an indicator of a tetragonal phase. For BT-70, there is a peak around 188 cm⁻¹, which is due to a slight amount of rhombohedral phase because it cannot be detected by crystal structure measurement,^[20] supported by X-Ray Diffraction (XRD) measurement in Figure S1, Supporting Information.

2.2. Electrical and Dielectric Performance of Composite Materials and TENG Devices

Figure 2 shows the mechanism of a triboelectric device using composite film and Al foil as negative and positive triboelectric materials, respectively. In brief, the TENG works due to a coupling effect between triboelectrification and electrostatic induction, that is, electrification furnishes static polarized charges, whereas the later converts mechanical energy to electricity during a periodic motion. In accordance with the triboelectric series,^[3] aluminum tends to lose electrons; meanwhile, PDMS tends to attract electrons. At the initial state in Figure 2a, there is neither charge transfer nor potential difference between the two layers. As compression is applied on aluminum (Figure 2b), $x(t)$ between aluminum and the composite film decreases from x_m to 0. Aluminum is positively charged, whereas the composite film is negatively charged due to electrification. The opposite triboelectric charges generated on each side reach the maximum. Once compression is released, with $x(t)$ increasing, negative charges on the composite film begin to induce positive charges on the opposite electrode due to the induction effect. So, electrons begin to flow from the bottom to top electrode in order to neutralize the positive triboelectricity, generating a positive voltage pulse, as shown in Figure 2c, till an equilibrium state is reached, as shown in Figure 2d. When compression is applied on aluminum again, electrostatic equilibrium is broken. With aluminum getting closer to the composite film, electrons flow back to the bottom, which generates a negative voltage pulse, as shown in Figure 2e.

Figure 2f displays the equivalent circuit model of an arbitrary TENG.^[4a] Electron flow is driven backward and forward through the external circuit when $x(t)$ between the two layers varies under mechanical force. From the $V-Q-x$ relationship equations^[4], output voltage of any TENG can be given by Equation (1):

$$V = -\frac{1}{C(x)}Q + V_{oc}(x) \dots \dots \dots (1)$$

The electrical potential of TENG contains two parts. $V_{oc}(x)$ is the voltage generated from the polarized triboelectric charges. Q is the transferred charges that contributes to the total electric potential. Q is influenced by the capacitance represented by $C(x)$. For contact-mode TENG, the output voltage equation can be given by Equation (2):

$$V = -\frac{Q}{S\varepsilon_0} \left(\frac{d}{\varepsilon_r} + x \right) + \frac{\sigma x}{\varepsilon_0} \dots \dots \dots (2)$$

where ε_0 , ε_r , σ , Q , S , x and d are vacuum permittivity, relative permittivity of the composite film, triboelectric charge density on the composite film, transferred charges at a certain x , surface area of the film, gap between the composite surface and aluminum, and thickness of the composite film, respectively. Capacitance between the two electrodes at a certain $x(t)$ for TENG can be obtained by Equation(3):

$$C(x) = \frac{\varepsilon_0 S}{x(t) + \frac{d}{\varepsilon_r}} \dots \dots \dots (3)$$

On the basis of this mechanism, output performance increases with an increase in relative permittivity ε_r or with a decrease in the effective thickness of the composite film. In this work, we chose the same kind of BT NPs with two different sizes to investigate the relative permittivity and triboelectric output performance of the composite film.

Figure 3 shows V_{oc} (open-circuit voltage) and I_{sc} (short-circuit current) of TENG using films filled with two different sizes of BT NPs under a periodic compression at a frequency of 2.8 Hz. Clearly, both V_{oc} and I_{sc} were found to be enhanced for TENG based on PDMS filled by both sizes of NPs. For TENG with pure PDMS, the peaks I_{sc} and V_{oc} were $\approx 6.9 \text{ mA m}^{-2}$ and $\approx 71 \text{ V}$, respectively. Output performance gradually enhanced as the mass ratio of BT NPs in the composite increased to 13 wt% for both samples. At 13 wt%, the peaks I_{sc} and V_{oc} for

BT-500/PDMS nanocomposites reached 41 mA m^{-2} and 103 V , whereas the values were 44 mA m^{-2} and 112 V for BT-70/PDMS nanocomposites, respectively. This feature suggests that the output signals for both sizes of BT NPs were almost the same. It was noted that output signals increased first and then decreased as a function of the filling content. As mass ratio of BT NPs further increased to 15 wt%, I_{sc} and V_{oc} decreased probably due to the exposed NPs on the PDMS surface;^[8] thus, effective contact surface area decreased for a high BT content.

Figure 4 shows V_{oc} , I_{sc} and charge density of TENG using different-sized BT NPs and MWCNT-filled BT-MWCNT/PDMS films under the same periodic compressive force at 2.8 Hz as before. For BT-500-MWCNTs/PDMS composites, the output performance gradually enhanced as the mass ratio of BT-500 is increased to 20 wt%. At 20 wt%, I_{sc} and V_{oc} peaks were 52 mA m^{-2} and 130 V , respectively, and the surface charge density was about 110 uC m^{-2} , which were higher than the values without MWCNTs. As to BT-70-MWCNT/PDMS composites, with the same mass ratio of BT-70 at 20 wt%, the peaks I_{sc} and V_{oc} were 65 mA m^{-2} and 150 V , respectively, which were much higher than the values of BT-500-MWCNT/PDMS. Furthermore, the optimum BT mass ratio of BT-70-MWCNT/PDMS composites was 25 wt%; the corresponding highest peaks I_{sc} and V_{oc} were 93 mA m^{-2} and 170 V , respectively, and the surface charge density was about 160 uC m^{-2} . It was worth noting that for both samples with 10 wt% BT and 1 wt% MWCNT the short current and transferred charges of BT-70-MWCNT/PDMS were higher than that of BT-500-MWCNT/PDMS, whereas the V_{oc} was lower than that of BT-500-MWCNT/PDMS. This may be because at 10 wt% BT with 1 wt% MWCNT, the dielectric loss of the sample with BT-70 was much higher than that with BT-500 during the motion frequency of 1-10 Hz

in Figure S3, Supporting Information. When the resistance of the external circuit was very large the triboelectric charges tend to be consumed inside the sample with time, leading to lower residual charges on the composite surface. From these results, it can be concluded that MWCNTs enhanced the size effect of BT NPs and showed better synergetic effect with smaller BT NPs on the triboelectric output performance. Meanwhile, the dielectric loss introduced by MWCNTs should also be considered and evaluated for later electric signal measurements.

Since PDMS has a high viscosity of 3500 centipoises, it may be hard to disperse fillers homogeneously even after long-time ultrasonic vibration, especially for nanofillers. As shown in Figure S2, Supporting Information, for the BT-70/PDMS composite with 13 wt% BT-70, there were many large clusters. We know that agglomeration and nanoparticle size in the composites were important for determining the final dielectric property. To avoid the adverse effect of aggregation and focus on the size effect, MWCNTs were chosen as functional material to improve the distribution of BT NPs. It has been reported that the addition of MWCNTs to the BT/PDMS composite not only avoided the aggregation of BT NPs but also increased the relative capacitance by increasing the effective (ϵ/d) value according to electromagnetism for conductive fillers.^[5b, 21] The same amount of 1wt% MWCNTs was added into BT/PDMS composite to ensure the same dispersion degree. The dielectric loss (See Figure S3, Supporting Information) of both films was is very low, which means that conductive MWCNTs formed discrete conductive micronetworks in the matrix, whereas small MWCNTs prevented the formation of conductive networks. In Figure S3, Supporting Information, for the BT-70-MWCNT/PDMS composite with 25 wt% BT-70 and 1wt%

MWCNT, no large clusters were observed. This indicates that BT NPs were uniformly surrounded by MWCNTs. The discrete conductive micronetworks filled with BT NPs are microcapacitor structures that contribute to the enhancement of effective filler-matrix interfacial area. Among the three-phase composites, the conductive MWCNTs also serve as a polarized charge transport phase for BT ferroelectric particles, increasing the charge storage ability of the matrix.

The theoretical BT NPs surface area and particle distance in a sample film (0.03 cm³) of BT-MWCNT/PDMS composite were evaluated, as shown in Figure 5, it was assumed that nanoparticles were homogeneously filled into a polymer matrix without aggregation. It is obvious that the surface area of BT NPs in both sizes increased with BT content. Compared with BT-500, BT-70 changed dramatically, leading to a much larger surface area. It has been reported that it exists a macroscopic region between the NPs and the matrix, which is different from the fillers and the matrix in character.^[14b] In this region, charge is injected from the NPs to the polymer matrix according to the electron affinity and equality of Fermi level or electrochemical potential,^[22] which induces ionization of particles and interfacial polymer matrix. Thus, a screening diffuse double layer is established called Gouy-Chapman diffuse layer.^[14b, 23] Considering a system with NPs of effective diameter d and interface of thickness t (Figure 5c), interfacial volume fraction f can be computed with Equation (4) Equation 4, where $2t/d < 1$:

$$f = 3 \frac{2t}{d} \left[1 - \left(\frac{2t}{d} \right) + \frac{1}{3} \left(\frac{2t}{d} \right)^2 \right] \dots \dots \dots (4)$$

Interface between BT NPs and PDMS polymer matrix is considered to have a finite thickness. According to Equation (4), when the interface thickness is in a certain value, as the

particle size decreases, the interfacial volume fraction increases. Smaller particles can afford larger total interfacial region, which can significantly enhance the electric displacement, D , of the composite film. From the particle distance curve in Figure 5b, it is clear that the inter-filler distance was roughly in the same order of magnitude as the nanofiller diameter for the content range of 10- 30 wt%. Smaller BT fillers lead to a smaller inter-filler distance, which may cause the interface of NPs to overlap more easily with the nearest neighbor NPs. This interface-overlapping phenomenon then may generate a collaborative effect among filler particles to intensify the interface effect on the macroscopic properties of nanocomposites.^[14b]

As electric displacement is proportional to the relative dielectric permittivity of the composite film, the dielectric properties of the composites with BT NPs in two different sizes before and after the addition of MWCNTs were investigated in the frequency range from 10^0 to 10^6 Hz at room temperature. As shown in Figure 6a-c, the dielectric constant of both composites increased with BT NPs. When BT content was <13 wt%, the difference in dielectric constant was not obvious, which explained the similar electrical property for the samples with different BT sizes. With an increase in the BT NPs content, the dielectric constant of the samples with BT-70 increased more rapidly than that with BT-500, which was in accordance with the slightly higher current density for composites with BT-70 than with BT-500. After adding MWCNTs, from Figure 6d-f, the dielectric constants for both composites were improved. It was worth mentioning that with the same amount of MWCNTs the dielectric constant of BT-70-MWCNT/PDMS was always much larger than that of BT-500-MWCNT /PDMS. As nanosized BT particles would tend to aggregate because of high surface energy and largely impairs the homogeneity of nanocomposites, without MWCNTs

the efficient interface area between BT and PDMS would be much less than the total BT surfaces, leading to negligible differences for different BT NPs sizes. Thus, the difference in electrical property is not noticeable between the samples with BT-70 and BT-500. With MWCNTs, the NPs reached a much better dispersion, thus, the efficient macroscopic interfacial region between BT NPs, MWCNTs and the PDMS matrix greatly increased. Consequently, the samples with BT-70 had higher electric displacement and relative dielectric permittivity. This explains why the current density of a BT-70-MWCNT/PDMS composite-based device may be higher than that of BT-500-MWCNT /PDMS for each BT content.

COMSOL Multiphysics simulation was performed to further confirm the surface potential difference introduced by the synergistic effects of BaTiO₃/ MWCNTs under two BT sizes. According to the transferred charge density(σ') equation:^[11]

$$\sigma' = \frac{\sigma d_{gap}}{d_{gap} + \frac{d_{film}}{\epsilon_r}} \dots \dots \dots (5)$$

where σ , d_{gap} , d_{film} and ϵ_r are triboelectric charge density at the equilibrium state, gap distance, film thickness, and dielectric constant of the composite film, respectively. For a certain TENG device, σ' is determined by both gap distance and dielectric constant of the films. During simulation, the same gap distance, film thickness and filler content of triboelectric layer are chosen. Hence, the analytical electric potential is derived by: $V_{oc} = \sigma' d_{gap} / \epsilon_0$. From figure 7, it is known that the transferred charge density σ' and electric potential V_{oc} of the BT-70-MWCNT/PDMS composite were higher than that of BT-500-MWCNT /PDMS under the same filler content.

The electrical output performance of TENG with optimized BT-70-MWCNT/PDMS

composite film was measured after connecting different resistances. When load resistance was $<1\text{ M}\Omega$, current and voltage signals did not change significantly (Figure 8a). With an increase in resistance from $0.5\text{ M}\Omega$ to $1\text{ G}\Omega$, the voltage (current) in the circuit rapidly increased (decreased). The maximum output power attained was $204\text{ }\mu\text{W cm}^{-2}$ under a load resistance of $20\text{ M}\Omega$. In Figure 8b, a device with 4 cm^2 area was used to charge different capacitors under a periodic pressure around 20 N force in 2.8 Hz . The power of TENG was sufficient to light up 60 Light Emitting Diodes (LEDs) when it was connected to a rectifying bridge circuit and $20\text{ M}\Omega$ load resistance actuated by slight hand tapping, as shown in Figure 8c.

3. Conclusion

The triboelectric output performance of TENG, based on BT-MWCNT/PDMS composites with two different sizes of BT (BT-70 and BT-500), was investigated. Results showed that for three-phase BT-MWCNT/PDMS composites, BT size influenced the triboelectric output performance of TENG. With the synergetic effect of MWCNTs, discrete microcapacitor structures formed. Composites with smaller-sized BT contributed to a higher interfacial area and larger electric displacement as verified by higher dielectric permittivity, resulting in better triboelectric output performance of TENG, as confirmed by COMSOL Multiphysics simulation. In addition, the optimal BT-70 mass ratio increased from 13 to 25 wt%, whereas from 13 to 20 wt% for BT-500. The optimal output current and voltage were 93 mA m^{-2} and 170 V , respectively, when the mass ratio of BT-70 NPs was 25 wt% (with 1 wt% MWCNTs), and the maximum charge density was around $160\text{ }\mu\text{C m}^{-2}$. The highest power density measured was $204\text{ }\mu\text{W cm}^{-2}$ when the load resistance was $20\text{ M}\Omega$. Moreover, the TENG can

instantaneously light up 60 commercial LEDs with a slight hand tapping. This work provides an insight into the necessity and ways of optimizing the microstructure of dielectric films in triboelectric applications.

4. Experimental Section

Composites and Devices: Two kinds of BT NPs were chosen for this study: 70 nm (BT-70; Alfa Aesar. NO.41633) and 500 nm in average particles (BT-500; Sigma Aldrich), as shown in Figure 1. First, BT NPs were dispersed in a PDMS elastomer (Sylgard 184; Dow Corning) with a weight ratio between 9 and 30 wt%. The BT/PDMS composite mixture with 20 mL chloroform solution was magnetically stirred for 4 h until the solution volatilized totally. Second, a curing agent was added followed by magnetic stirring for another 20 min. After degassing in vacuum for 20 min, the mixture was cast onto a petri dish and cured at 80 °C for 2 h. For BT-MWCNT/PDMS composite films, MWCNTs (purity >98%, OD 20-30 nm, length 10-30 μm ; Timesnano) with a weight ratio of 1 wt% were chosen, using the same process. The film thickness was 300 μm in average. Finally, the composite film was peeled off. For the TENG device, acrylic plates were chosen as substrates. An aluminum foil was prepared as top electrode and positive triboelectric material. The composite film acted as the negative triboelectric material with bottom electrode of copper foil. The area of the contact surface was 1 cm^2 .

Characterization: SEM (LEO Gemini 530) was utilized to conduct the morphology characterization of BT NPs and composite films. A D2 Phaser X-ray Powder diffractometer (Bruker) and Raman spectroscopy (model HR Evaluation; LabRAM) with a source

wavelength of 514 nm were used for the phase analysis of BT NPs. The dielectric properties of composites were characterized with an impedance analyzer (Solatron ModuLab XM MTS). For testing the power generation by TENG, a linear motor system was setup as mechanical source for periodic motions (in Figure S4, Supporting Information). The TENG output was measured at a working frequency of 2.8 Hz and a periodic pressure of 0.2 MPa. The electrical signals of TENG were measured with an electrometer (Keithley 6514) and an oscilloscope (Wavejet 354A, Lecroy).

Acknowledgements

Shan Feng thanks the financial support from the China Scholarship Council (Scholarship file no. 201506410057). The authors also acknowledge Mr. Éric Perrin for his help in setting up the linear motor systems.

References

- [1] N. L. Panwar, S. C. Kaushik, S. Kothari, *Renew. Sust. Energ. Rev.* **2011**, *15*, 1513-1524.
- [2] a) F. R. Fan, Z. Q. Tian, Z. L. Wang, *Nano Energy* **2012**, *1*, 328-334; b) H. Hwang, K. Y. Lee, D. Shin, J. Shin, S. Kim, W. Choi, *Appl. Surf. Sci.* **2018**, *442*, 693-699.
- [3] Z. L. Wang, *ACS Nano* **2013**, *7*, 9533-9557.
- [4] a) S. Niu, S. Wang, L. Lin, Y. Liu, Y. S. Zhou, Y. Hu, Z. L. Wang, *Energ. Environ. Sci.* **2013**, *6*, 3576; b) S. Niu, Z. L. Wang, *Nano Energy* **2015**, *14*, 161-192.
- [5] a) K. Y. Lee, J. Chun, J. H. Lee, K. N. Kim, N. R. Kang, J. Y. Kim, M. H. Kim, K. S. Shin, M. K. Gupta, J. M. Baik, *Adv. Mater.* **2014**, *26*, 5037-5042; b) X. He, H. Guo, X. Yue, J. Gao, Y. Xi, C. Hu, *Nanoscale* **2015**, *7*, 1896-1903; c) J. Chun, J. W. Kim, W. S. Jung, C. Y. Kang, S. W. Kim, Z. L. Wang, J. M. Baik, *Energ. Environ. Sci.* **2015**, *8*, 3006-3012.
- [6] A. F. Diaz, R. M. Felix-Navarro, *J. Electrostat.* **2004**, *62*, 277-290.
- [7] a) Z. Pan, L. Yao, J. Zhai, B. Shen, H. Wang, *Compos. Sci. Technol.* **2017**, *147*, 30-38; b) Y. Bai, Z. Y. Cheng, V. Bharti, H. Xu, Q. Zhang, *Appl. Phys. Lett.* **2000**, *76*, 3804-3806; c) P. Kim, N. M. Doss, J. P. Tillotson, P. J. Hotchkiss, M. J. Pan, S. R. Marder, J. Li, J. P. Calame, J. W. Perry, *ACS Nano* **2009**, *3*, 2581-2592; d) R. Schroeder, L. A. Majewski, M. Grell, *Adv. Mater.* **2005**, *17*, 1535-1539.
- [8] J. Chen, H. Guo, X. He, G. Liu, Y. Xi, H. Shi, C. Hu, *ACS Appl. Mater. Interfaces* **2016**, *8*, 736-744.

- [9] Y. H. Kwon, S. H. Shin, Y. H. Kim, J. Y. Jung, M. H. Lee, J. Nah, *Nano Energy* **2016**, *25*, 225-231.
- [10] N. Soin, P. Zhao, K. Prashanthi, J. Chen, P. Ding, E. Zhou, T. Shah, S. C. Ray, C. Tsonos, T. Thundat, E. Siores, J. Luo, *Nano Energy* **2016**, *30*, 470-480.
- [11] Z. Fang, K. H. Chan, X. Lu, C. F. Tan, G. W. Ho, *J. Mater. Chem. A* **2018**, *6*, 52-57.
- [12] a) T. Hanemann, D. V. Szabó, *Materials* **2010**, *3*, 3468-3517; b) R. Eglitis, D. Vanderbilt, *Phys. Rev. B* **2007**, *76*, 155439; c) R. I. Eglitis, *Appl. Surf. Sci.* **2015**, *358*, 556-562.
- [13] M. Frey, D. Payne, *Phys. Rev. B* **1996**, *54*, 3158.
- [14] a) Z. M. Dang, J. K. Yuan, S. H. Yao, R. J. Liao, *Adv. Mater.* **2013**, *25*, 6334-6365; b) T. Tanaka, M. Kozako, N. Fuse, Y. Ohki, *IEEE Trans. Dielectr. Electr. Insul.* **2005**, *12*, 669-681.
- [15] a) Y. Mao, S. Mao, Z. G. Ye, Z. Xie, L. Zheng, *J. Appl. Phys.* **2010**, *108*, 014102; b) W. Yang, S. Yu, S. Luo, R. Sun, W. H. Liao, C. P. Wong, *J. Alloy. Compd.* **2015**, *620*, 315-323; c) Y. Kobayashi, T. Tanase, T. Tabata, T. Miwa, M. Konno, *J. Eur. Ceram. Soc.* **2008**, *28*, 117-122.
- [16] X. He, H. Guo, X. Yue, J. Gao, Y. Xi, C. Hu, *Nanoscale* **2015**, *7*, 1896-1903.
- [17] G. Wang, Y. Xi, H. Xuan, R. Liu, X. Chen, L. Cheng, *Nano Energy* **2015**, *18*, 28-36.
- [18] a) S. Wang, L. Lin, Z. L. Wang, *Nano Lett.* **2012**, *12*, 6339-6346; b) Y. P. Jeon, J. H. Park, T. W. Kim, *Appl. Surf. Sci.* **2018**, *445*, 50-55.
- [19] S. Valencia, A. Crassous, L. Bocher, V. Garcia, X. Moya, R. Cherifi, C. Deranlot, K. Bouzehouane, S. Fusil, A. Zobelli, *Nat. Mater.* **2011**, *10*, 753.
- [20] C. H. Perry, D. B. Hall, *Phys. Rev. Lett.* **1965**, *15*, 700-702.
- [21] X. Yang, W. A. Daoud, *J. Mater. Chem. A* **2017**, *5*, 9113-9121.
- [22] M. Saint Jean, S. Hudlet, C. Guthmann, J. Berger, *Eur. Phys. J. B* **1999**, *12*, 471-477.
- [23] J. Wang, F. Guan, L. Cui, J. Pan, Q. Wang, L. Zhu, *J. Polym. Sci., Part B: Polym. Phys.* **2014**, *52*, 1669-1680.

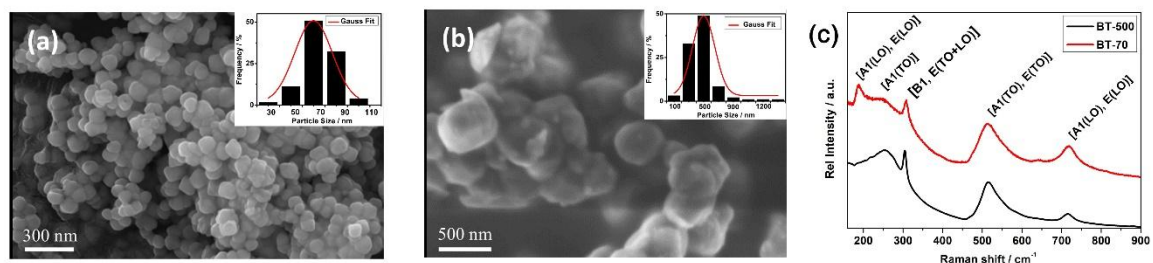


Figure 1 SEM images of a) BT-70 and b) BT-500. c) Raman Spectra of BT-70 and BT-500. The insets in (a) and (b) are histograms of the measured particle sizes. The solid line is the Gauss fit curve.

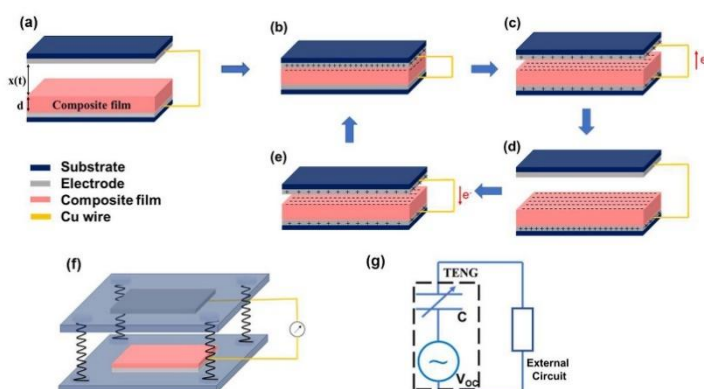


Figure 2 a-e) Charge generation mechanism of the TENG under an external force. f) Schematic structure diagram of TENG device. g) Equivalent circuit model of any TENG.

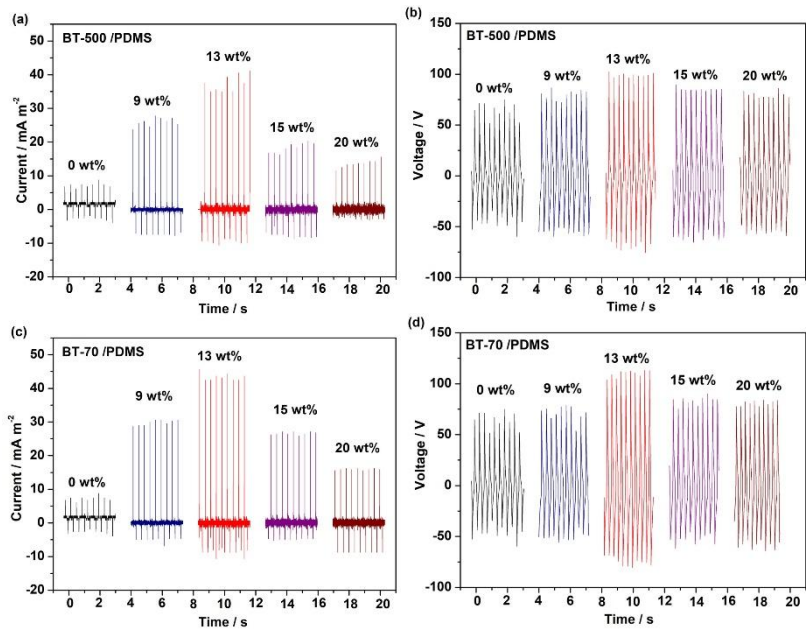


Figure 3 a,c) Output current, and b,d) voltage of TENG using BT/PDMS nanocomposite films with different BT sizes and mass ratios, measured at a frequency of 2.8 Hz.

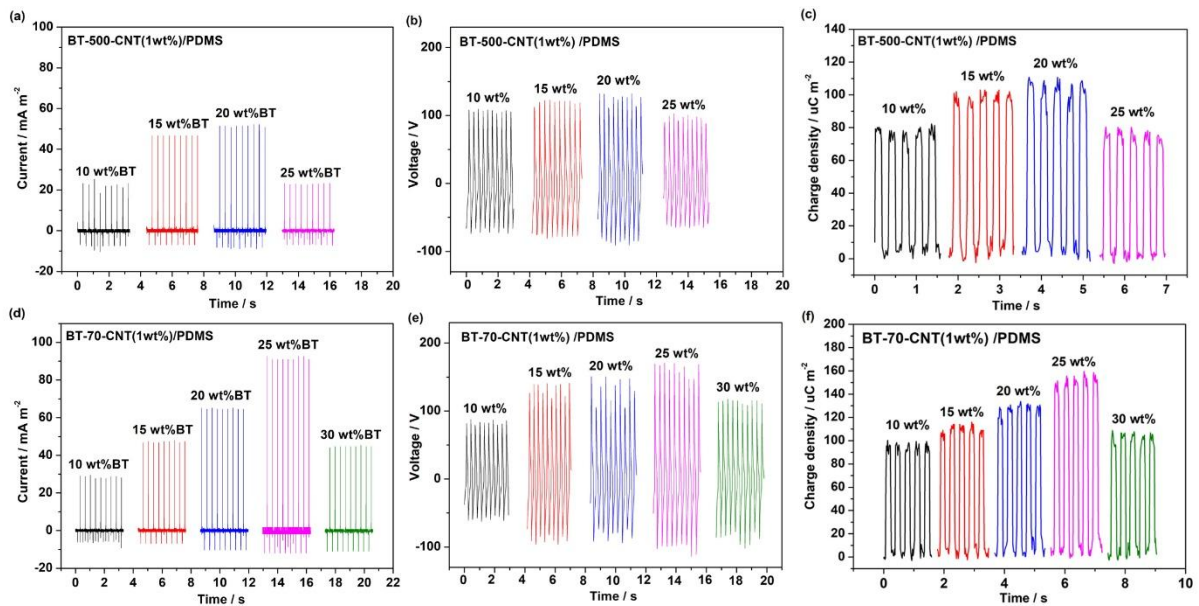


Figure 4 a,d) Output current, b,e) voltage, and c,f) charge density of TENG using BT-MWCNT/PDMS nanocomposite films with different BT sizes and mass ratios, measured at a frequency of 2.8 Hz.

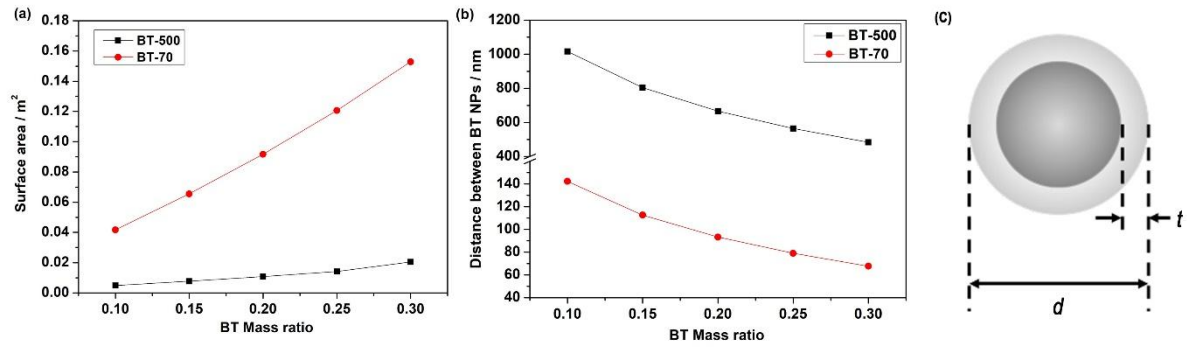


Figure 5 a) Theoretical BT NPs surface area. b) Interparticle distance in the BT-MWCNT/PDMS composite with 1 wt% MWCNTs; c) A nanoparticle with interfacial polymer layer.

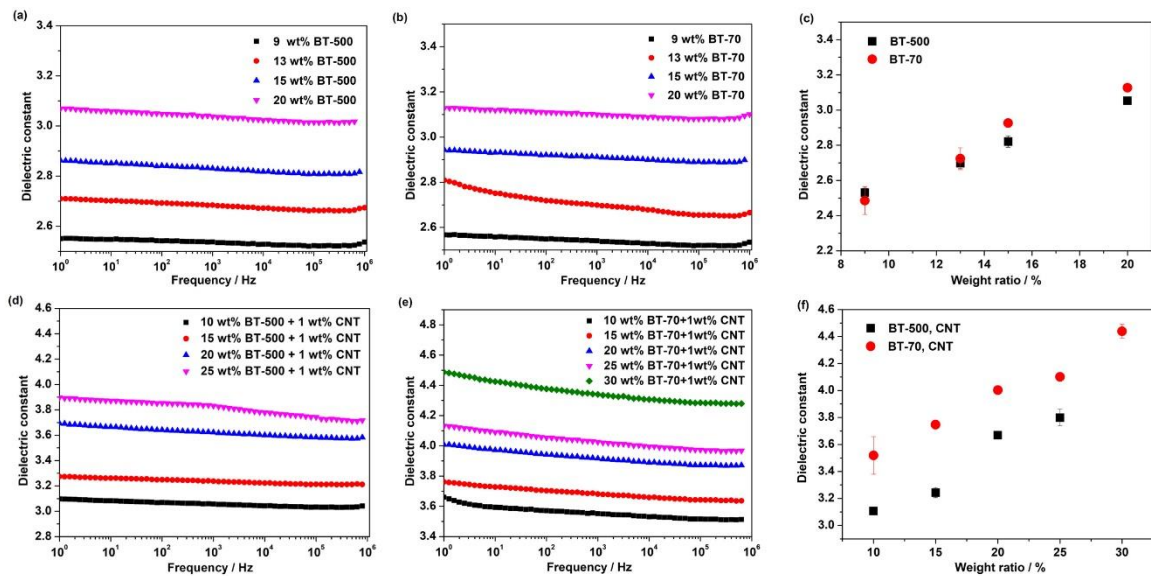


Figure 6 Dependence of dielectric constant of the composite films with different filler contents on frequency in the range of $10^0 - 10^6$ Hz for: a) BT-500/PDMS films and b) BT-70/PDMS films. c) Comparison between BT-500/PDMS and BT-70/PDMS films with different BT weight ratios. d) For BT-500/PDMS films with 1wt% MWCNTs. e) For BT-70/PDMS films with 1wt% MWCNTs. f) Comparison between BT-500-MWCNT/PDMS and BT-70-MWCNT/PDMS films with different BT weight ratios.

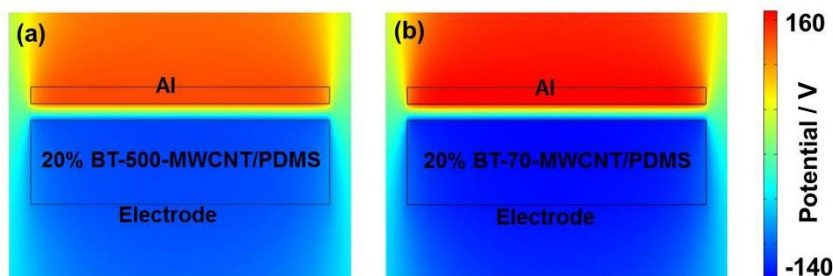


Figure 7 COMSOL simulation results of triboelectric potential difference.

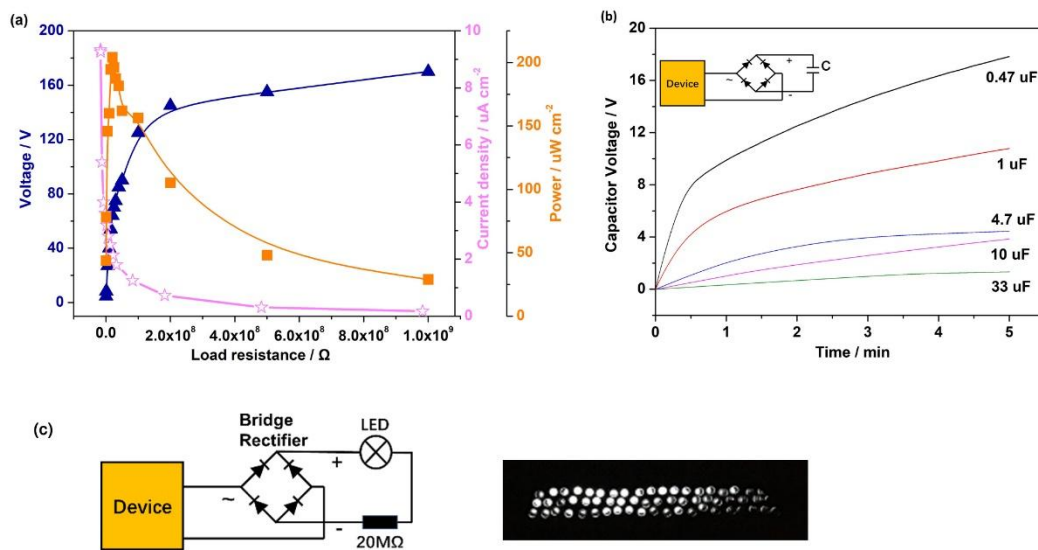


Figure 8 a) Maximum output voltage, current and power under different external loads. b) Charging different capacitors under a periodic pressure around 20 N force in 2.8 Hz. c) White LEDs lit by TENG under hand tapping.



Shan FENG received her B.S. and M.S. degree in Materials Science and Engineering from China University of Geosciences, under the supervision of Prof. Jin TAN. Now she is a CSC sponsored Ph.D candidate directed by Prof. Jinbo Bai at University of Paris-Saclay, France. Her research mainly focuses on dielectric material synthesis and characterization, fabrication of triboelectric nanogenerators.

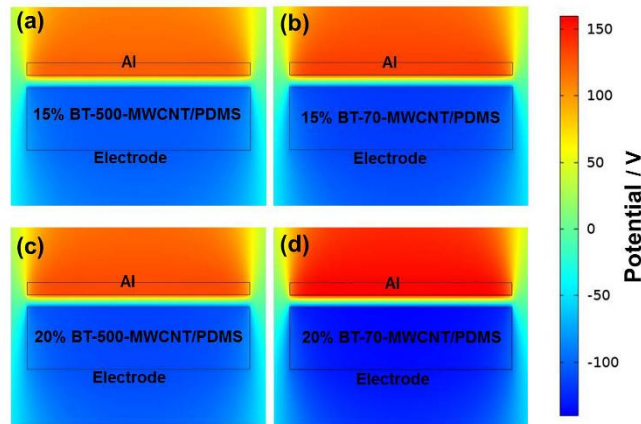


Delong He received his Ph.D. degree in materials science from Ecole Centrale Paris (France) in 2010. He conducted Post-doc research at CEA-Saclay in 2011 and then at CNRS MSSMat laboratory from 2012 to 2013. Since 2016, he is permanent research engineer of Ecole CentraleSupélec (France). His research interests are multifunctional composite materials and energy.



Jinbo Bai received his Master degree of Solid Mechanics from Xi'an Jiaotong University in 1985 and Ph.D. degree of Science of Materials from Ecole Centrale Paris in 1991. He was lecturer of Mechanics of Materials in Northwestern Polytechnic University 1985–1987 and CNRS Researcher then Director of research in Lab. MSSMAT, UMR8579 of Ecole Centrale Paris since 1991. His research interest cover from nuclear materials Zr&Ti, hydrogen storage and embrittlement, composites materials, micromechanical modelling, finite element simulations, carbon nanomaterials' syntheses, characterizations and applications, structural and multi-functional nano/microcomposites, hybrid fillers, heat management, energy storage and green energy in general.

Table of Contents Graphic



Brief Summary

Triboelectric nanogenerators based on the BT-MWCNT/PDMS composite films are designed at different BaTiO₃ size and mass ratio. Synergistic effects of BaTiO₃/MWCNT fillers on the triboelectric output performance have been studied. As to BT-70-MWCNT/PDMS composites, with the same mass ratio of BT, the peak output current is always higher than that of BT-500-MWCNT/PDMS.

Key word: triboelectric nanogenerator